Numerical Simulation of Atmospheric Passage of Interplanetary Dust Particles

Tyler Gonzales
Dr. Paul Thomas and Dr. Philip Ihinger

Abstract
Numerical methods have been utilized in applied mathematics and physics for decades. The numerical simulation of trajectories of particles is an interesting topic to many professionals including physicists, mathematicians, and geochemists. Quite frequently, interplanetary dust particles fall to Earth's surface and can be separated from terrestrial dust and analyzed. In this project, we develop a Python-based numerical model, which relies on the finite difference method (FDM). Our numerical simulation results show that atmospheric deceleration for micrometeorites occurs at high altitudes (80 km) and converts sufficient kinetic energy to heat that can potentially melt the micrometeorites entirely, a result consistent with laboratory analysis of recovered samples.

Keywords
Micrometeorites, Numerical Simulation, Finite Difference Method, Atmospheric Entry

[1] *Graduate Institutional Affiliation: Applied Mathematics Program, Yale University*
*__Corresponding author__: tyler.gonzales@yale.edu

Contents

1. Introduction

Micrometeorites (see Figure 1 and 2) are interplanetary dust particles that offer important insights into Earth's origin and the nature of our solar system. They are tiny rock bodies that range from roughly 50 μm to 2 mm in diameter. There are numerous methods that have been used to collect and analyze such stones. [15].

Until recently, much was unknown about such meteorites and how their trajectories interplay with their chemical composition and physical characteristics. In fact, the development of a complete geochemical analysis of micrometeorites remains a goal of scientists to this day. There have been models developed for meteorites that are not on a micro-scale, however, and it should be pointed out that [2, 8, 9] are great sources for those interested in other astrophysical models.

Figure 1. Micrometeorites collected from urban rooftops [15].

In this article, we develop a Python-based trajectory model for the atmospheric passage of micrometeorites of various sizes with the aim of comparing our results with the observable data that is already known about meteorites. The simulation is based on the finite-difference method (FDM), a numerical technique that can be used to solve complicated systems of differential equations. Though other more complicated techniques can be used to solve some Partial Differential Equations (PDE), such as the finite element method (FEM), FDM is a suitable numerical technique which produces satisfactory results

while requiring less computational sophistication.

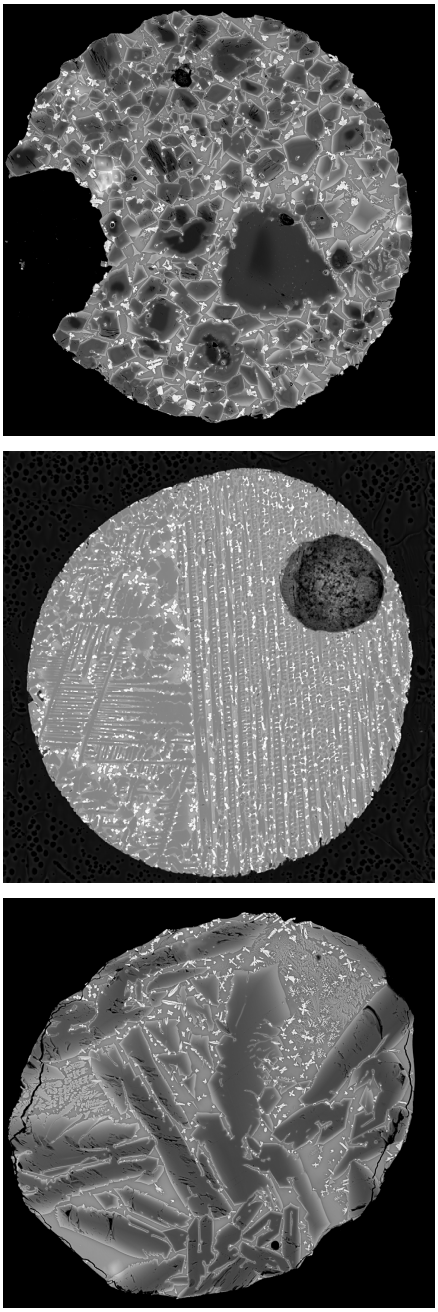

Figure 2. Photomicrographs of micrometeorites. Images taken by Dr. Anette von der Handt at the microprobe facility in the Department of Earth and Environmental Sciences at the University of Minnesota. Micrometeorite samples collected by Scott Peterson of New Hope, MN. Variations in crystal sizes and shapes reflect different thermal histories for the meteorites.

The following sections are organized as follows: in Section 2, a discussion of the needed physics and governing equations of motion is provided, followed by definitions of parameters used in the model. In Section 3, we discuss the density model used in this simulation. Section 4 outlines the theory behind FDM, and how we apply this technique to the equations of motion for our simulations. In Sections 5 and 6, we present simulations of large-sized objects and micrometeorite-sized objects, respectively. In Section 7 we discuss a preliminary heating model. The final section of this paper includes a closing discussion of the findings, as well as some possibilities for future work and acknowledgements.

2. Input Physics

Classic trajectory equations, which explain both change in velocity with time and change in angle of atmospheric entry with time, are

$$m\frac{dv}{dt} = -\frac{1}{2}C_D\rho_a A v^2 + mg\sin\theta, \tag{1}$$

$$\frac{d\theta}{dt} = \frac{g\cos\theta}{v} - \frac{C_L\rho_a A v}{2m} - \frac{v\cos\theta}{R_p + z}, \tag{2}$$

where the angle of the trajectory θ is measured from the horizontal (for example, a vertical trajectory corresponds to an angle of 90 degrees). In (1) the term $-\frac{1}{2}C_D\rho_a A v^2$ accounts for (quadratic) drag on the object, which includes constants C_D (the drag coefficient), ρ_a (atmospheric density), and A (cross-sectional area of the object). The second term in (1) represents a gravitational acceleration component.

In (2) the first term is a gravity component, the second is a lift term including C_L (the lift coefficient), and the third term takes into account the sphericity of the gravitational field associated with Earth. Together, (1) and (2) give the basis of a trajectory model that can be solved using numerical schemes, such as FDM.

When entering the atmosphere, the micrometeorites interact with air particles, causing the rock to heat up upon entry. Once the energy is transferred to the micrometeorites, their temperature will rise. This heating and interaction of particles can lead to ablation, which is generally written as a mass-loss equation [5]

$$Q\frac{dm}{dt} = -A\min\left(\frac{1}{2}C_H\rho_a v^3, \sigma T_{\max}^4\right). \tag{3}$$

In (3), Q (the heat of ablation) is a variable depending on material type and ablative process, and C_H is the heat-transfer coefficient. Values of Q for various types of micrometeorites are given in Table 1 [8]. The first component of the minimum in (3),

$$Q\frac{dm}{dt} = -A\frac{1}{2}C_H\rho_a v^3,$$

Table 1. Parameters for Micrometeorites [8]

Type	Density (kg m^{-3})	Velocity (m s^{-1})	Q (MJ kg^{-1})
Iron	7900	15,000	8.0
Stone	3500	15,000	8.0
Carbonaceous	2200	15,000	5.0
Short Period Comet	1000	25,000	2.5

is a valid ablation model for higher altitudes in the atmosphere (this is where most meteorites would burn up and form the so-called *meteor trails* [5] we can sometimes see in the sky). However, for lower altitudes, say $z < 30$ km, we need an ablation model that accounts for the increased amount of kinetic energy which is absorbed as a result of ionized gas at the shock front of atmospheric entry. These temperatures are extremely high (around 25,000 K), and so the maximum ablation rate at these temperatures is given by

$$Q\frac{dm}{dt} = -A\sigma T_{\text{max}}^4,$$

where σ is the Stefan-Boltzmann constant $\sigma = 5.676 \times 10^{-8}$ $\text{Wm}^{-2}\text{K}^{-4}$ and $T_{\text{max}} = 25,000$ K [3].

The term σT_{max}^4 comes from radiative heating of the micrometeorite, which involves ideas from thermal radiation. We introduce a term $q^{(e)}$, which is the energy emitted (from a *black body*) per unit area per unit time. The *Planck Distribution Law* gives an expression for the energy emitted by a blackbody as a function of both wavelength and temperature [14]:

$$q_{b\lambda}^{(e)} = \frac{2\pi c^2 h\lambda^{-5}}{\exp\left(\dfrac{ch}{k_B\lambda T}\right) - 1}.$$

Here, $c = 3.0\times10^8$ ms^{-1} (the speed of light), $h = 6.624\times 10^{-27}$ erg s (Planck's constant), and $k_B = 1.380 \times 10^{-16}$ erg K^{-1} (Boltzmann's constant).

The total emissive energy of a black body can therefore be determined by integrating the Planck distribution law over wavelengths $0 \le \lambda < \infty$:

$$q_b^{(e)} = \int_0^\infty q_{b\lambda}^{(e)}\, d\lambda = \int_0^\infty \frac{2\pi c^2 h\lambda^{-5}}{\exp\left(\dfrac{ch}{k_B\lambda T}\right) - 1}\, d\lambda.$$

Upon evaluation of this integral, we see find that the total emissive energy of a blackbody is

$$q_b^{(e)} = \frac{2\pi^5 k_B^4 T^4}{15c^2h^3} = \sigma T^4.$$

Replacing T with $T_{\max}$ in this equation gives our maximum ablation rate under high temperatures, as in (3).

When considering heat flow for the micrometeorites, there is the heat due to ablation and radiation, and the internal heating of the micrometeorite with time. The following discussion is about the internal heating of the micrometeorite during its fall through the atmosphere. Heat flow in three-dimensions - for isotropic materials - and heat-flux are related through Fourier's law of conduction [14]

$$\mathbf{q} = -k\nabla T, \tag{4}$$

where k is the thermal conductivity, or a measure of ability to conduct heat, and ∇T is the temperature gradient. Typical units for this k are in $\text{Wm}^{-1}\text{K}^{-1}$.

A solution to (4) would be a temperature distribution in spatial coordinates. Temperatures are frequently time-dependent quantities, and the temperature at a future time and coordinate in space is a solution of the heat equation

$$\frac{\partial T}{\partial t} = \alpha\nabla^2 T = \alpha\Delta T, \quad \alpha = \frac{k}{\rho C_v}$$

where α is the thermal diffusivity; this quantity measures the rate of heat transfer through a material (ρ_m and C_v are the density and specific heat of the material, respectively).

We can compare the rate of heat conduction with the micrometeorite to the ablation rate of the surface of the rock. The rate of heating of a the surface is approximately [19]

$$\kappa_H = \frac{k}{\rho_m C_p},$$

where C_p is the heat capacity of the object. Assuming the surface temperature is T_0 and the internal of the rock is $T = 0$, then the temperature at future all time increments at a radial distance r inside the micrometeorite is given via the integral equation

$$T(r,t) = \frac{2T_0}{\sqrt{\pi}} \int_{\frac{r}{2}(\kappa_H t)^{-1/2}}^{r} \exp(-\mu^2)\, d\mu.$$

We can directly solve the integral equation using a readily available solver. The resulting solution will give us a temperature distribution as a function of time and location within micrometeorite.

The amount of drag and heating experienced on the micrometeorite depends on the atmospheric density at various heights. Though approximate models exist for atmospheric density (in terms of simple exponential functions), more realistic models use interpolation to approximate values of atmospheric density at given heights for the most accurate results.

3. Atmospheric Density Considerations

A large factor in this simulation, and every astrophysical model which involves an atmosphere, is the best way to account for atmospheric density. This is a rather difficult task, as the density is not uniform with height. Rather, the atmospheric density varies with height, temperature, and location. We use the *COSPAR International Reference Atmosphere* (CIRA) as the foundation of our atmospheric model.

The CIRA models are developed by the Committee on Space Research (COSPAR) and are widely respected models that are used in preparations for space flight. We can use the data provided in the CIRA model to approximate the density of the atmosphere up to 180 km. To do so, we consider a combination of a seventh-order polynomial approximation with a function inside an exponential function of altitude z. This results in the approximation

$$\rho_a(z) \simeq 10^{\,f_\rho(z)},$$

where $f_\rho(z) = a_0 + a_1 z^1 + \cdots + a_7 z^7$. The coefficients a_i $(1 \leq i \leq 7)$ depend on the recorded data in CIRA.

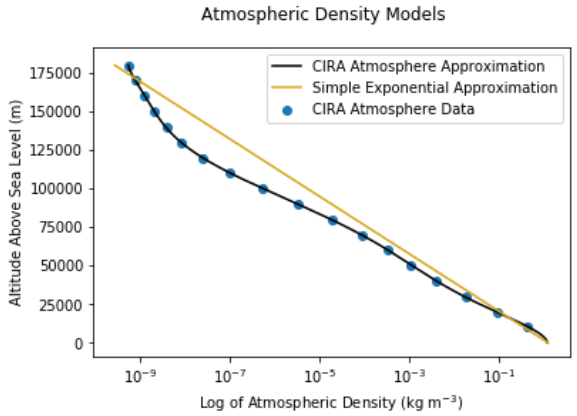

Figure 3. Log of density plot comparing the CIRA model and a simple exponential approximation.

The coefficients for the approximation are provided in Table 2. This seventh-order approximation technique was originally developed by the Air Force Geophysics Lab in 1985 [13].

Figure 3 compares the best-fit of the CIRA data to the simple exponential model. The CIRA data deviate noticeably from the simple exponential atmospheric model at altitudes of greater than 75 km. We show that applying the more accurate model (or the fit to the CIRA data) results in significant differences in the trajectories and thermal histories of micrometeorites. Though using a simple exponential decay model for atmosphere $\rho_a(z) \simeq \rho_0 \exp(-z/H)$, where H is the scale height, is appropriate for models which do not involve high altitude considerations, we need the additional complexity and realism obtained by using the CIRA data to obtain the most realistic simulation results.

Table 2. Coefficients for the Polynomial Approximation

Coefficient	Value
a_0	7.001985×10^{-2}
a_1	-4.336216×10^{-3}
a_2	-5.009831×10^{-3}
a_3	1.621827×10^{-4}
a_4	-2.471283×10^{-6}
a_5	1.904383×10^{-8}
a_6	$-7.189421 \times 10^{-11}$
a_7	1.060067×10^{-13}

4. Numerical Techniques

The primary tool used in developing the model is FDM. This technique is used to approximate the derivative of a function using a sequence of finite differences. In this section, we briefly explain this method. The derivative $f'(t)$ of a function $f(t)$ can be approximated via the finite difference

$$f'(t) = \frac{df}{dt} \simeq \frac{f(t+\Delta t) - f(t)}{\Delta t}.$$

Given our trajectory equations, we can apply this finite difference scheme to obtain a discretized set of equations modeling the trajectory of an object of mass m. Take, for example, (1). We can apply the finite-difference approximation

$$\frac{dv}{dt} \simeq \frac{v(t+\Delta t) - v(t)}{\Delta t}$$

to (1). After multiplying through by mass, the approximation is

$$m\frac{dv}{dt} = -\frac{1}{2}C_D\rho_a A v^2 + mg\sin\theta \simeq m\frac{v(t+\Delta t) - v(t)}{\Delta t}.$$

Dividing both sides by m gives

$$-\frac{1}{2m}C_D\rho_a A v^2 + g\sin\theta \simeq \frac{v(t+\Delta t) - v(t)}{\Delta t}$$

so that

$$v(t+\Delta t) = v(t) - \frac{C_D\rho_a A v^2 \Delta t}{2m} + g\Delta t\sin\theta. \quad (5)$$

Similarly, we can obtain formulae for discretized angle and mass relationships. After applying FDM to (2) and (3), we obtain the relationships

$$\theta(t+\Delta t) = \theta(t) + \frac{g\Delta t\cos\theta}{v} - \frac{C_L\rho_a A v\Delta t}{2m} - \frac{v\Delta t\cos\theta}{R_p + z} \quad (6)$$

and

$$m(t+\Delta t) = m(t) - \frac{A\Delta t}{Q} \min\left(\frac{1}{2} C_H \rho_a v^3, \sigma T_{\text{max}}^4\right). \quad (7)$$

Height at each step can also be determined using

$$z(t+\Delta t) = z(t) - v\Delta t \sin\theta.$$

In general, given a time-dependent function $\gamma(t)$, we think of $\gamma(t+\Delta t)$ representing the function γ at the new (updated) time value $t+\Delta t$, giving the updated value of γ at each point along the process. The quantity Δt is known as the time-step, and is set at the beginning of the simulation. Therefore, in (4), (5), and (6), the quantity on the left side of each equation should be thought of as the new value obtained through finite-difference steps, while the value on the right is the previous value in the iteration.

We will refer to (5), (6), and (7) as the discretized (finite-difference) equations of motion for a particle of mass m. Since the original differential trajectory equations are complicated, and mass is not constant, we choose to employ these finite-difference techniques to solve the original equations of motion. The benefit of numerical solutions is that the discretized equations of motion are able to be imported directly into Python and solved using computational tools.

5. General Simulations

Since the idea of micrometeorites still may seem foreign to some readers, we figure a discussion on some of the physical behavior (and intuition) behind atmospheric entry would be best suited in the case of larger objects. Parameters for these simulations are included in Table 3.

Table 3. Parameters for Initial Simulations

Parameter	Value	Units
Scale Height (H)	8100	m
Heat of Ablation (Q)	8×10^6	Jkg^{-1}
Drag Coefficient (C_D)	1.7	N/A
Lift Coefficient (C_L)	1×10^{-3}	N/A
Heat Transfer Coefficient (C_H)	0.1	N/A

As a remark on two of the coefficients in Table 3, C_H was determined from photographic evidence of meteors [5], and C_L was observationally determined as well [18]. These numerical values do not actually change much from object to object, so these will remain consistent throughout. The simulations were ran with a step-size of $\Delta t = .01$ s.

From these first plots we can make a couple of interesting comments. First, note that most of the kinetic

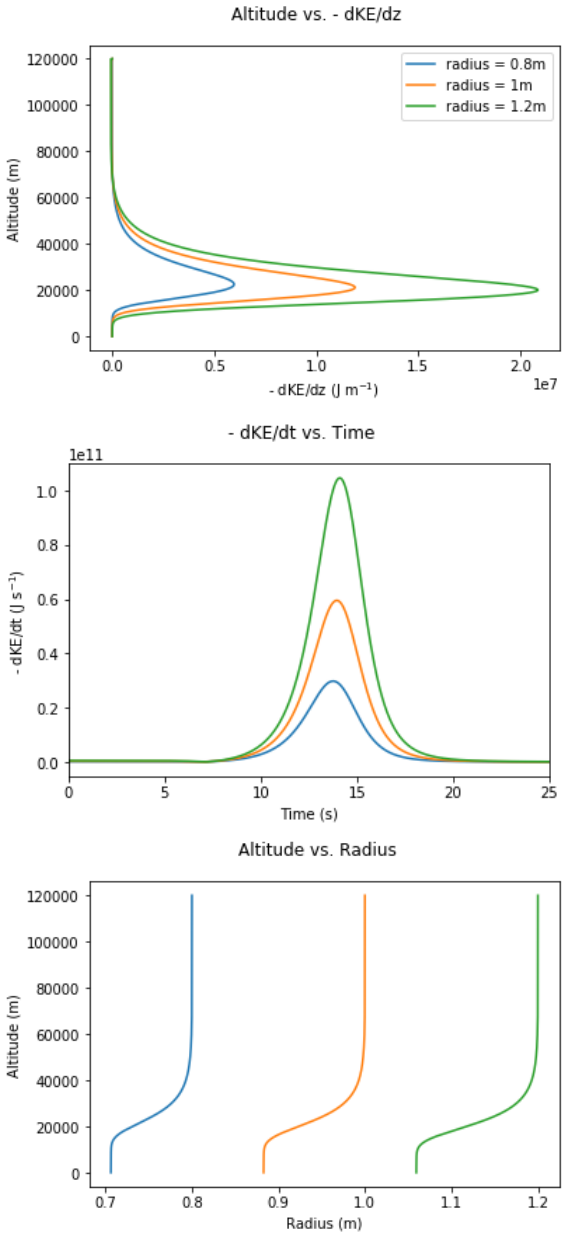

Figure 4. Results for a general simulation showing kinetic energy dispersion into the atmosphere, kinetic energy loss with time, and ablation with altitude.

energy is dispersed at altitudes of just above 20 km for meteorites with radii on the order of 1 m. Second, the time span of this loss would be no greater than 10 s. We can also approximate an order of magnitude analysis on heating for meteorites from these plots, but we will do so just for micrometeorites in the next section. We also produce simulations that model ablation, change in

speed, and angle, with height. Recall that this is done by running FDM on (1), (2), and (3).

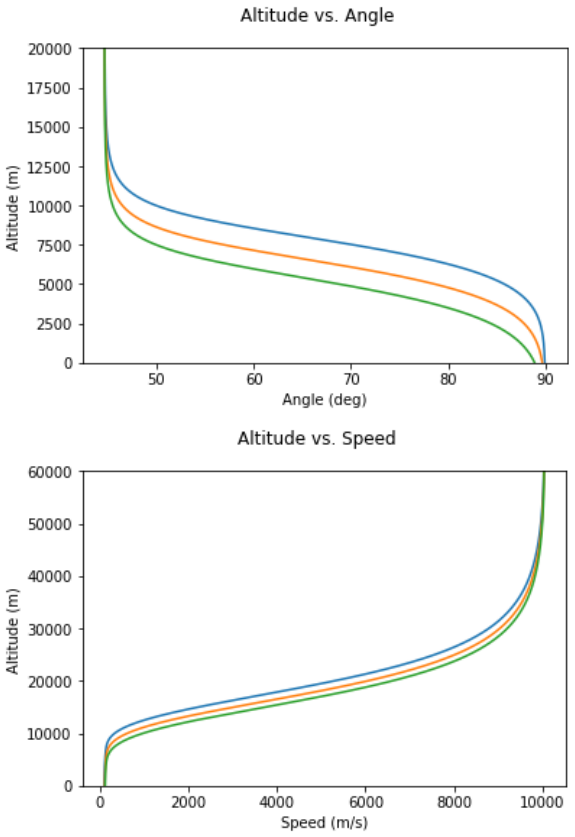

Figure 5. Results for a general simulation showing change in angle and change in speed with time. Legends for these plots correspond to the legend given in Figure 3.

Figure 5 shows that ablation of small meteorites begins at around 40 km, and the angle fluctuates from an initial entry angle of 45 degrees to the horizon to a completely vertical trajectory. The meteorites reach terminal velocity at under 10 km. Another simulation, which is not shown here, show that these larger rocks take from around 80 s to 100 s to reach $z = 0$ m.

6. Micrometeorite Simulation Results

The overall goal of the numerical model is a simulation for micrometeorites, and comparing the results obtained here for larger sized meteorites from the previous section. Since simulations involving very small data values can be computationally expensive for our differential equations, we need to investigate a stopping condition for our simulation that does not cause us to lose any of the important physics. The largest infinitesimal change in kinetic energy with change in height occurs at high altitudes greater than 60 km micrometeorites, so we can assume most of the important data we need will also occur at these altitudes. For this reason, we end the simulation once the velocity reaches terminal velocity. That is,

$$v = \sqrt{\frac{2mg}{\rho_a A C_D}}.$$

Though this stopping condition makes physical sense, it turns out it is still rather computationally expensive. After running a couple of simulations, it can be shown that we can stop the finite difference calculations at approximately terminal velocity, or heights where this value is obtained.

For these simulations, a time step of $\Delta t = .01$ was used, and parameters for micrometeorites are the same as those in Table 2. The stopping condition for these simulations will be set to end once a height of 50 km is reached, it can be shown that this is essentially the height at which terminal-velocity is reached for the micrometeorites in this model, as the results will show.

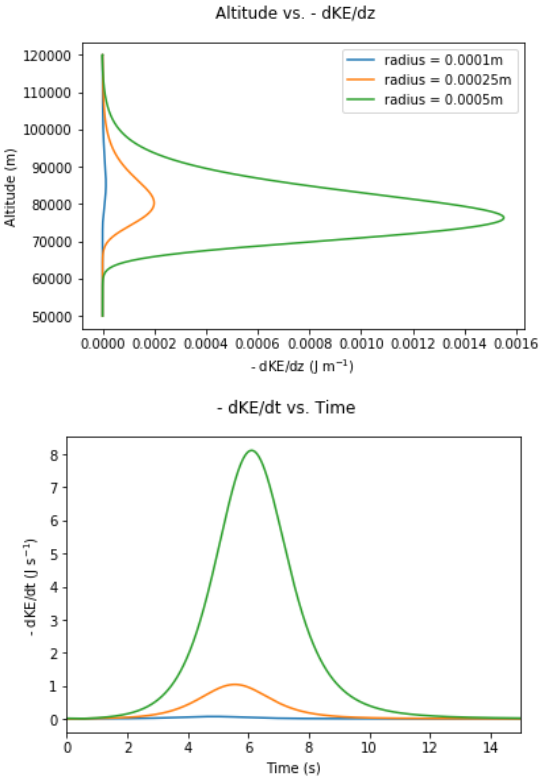

Figure 6. Results for a micrometeorite simulation showing kinetic energy dispersion into the atmosphere and kinetic energy loss with time.

Notice how much higher ablation begins to occur here than with larger meteorites, ablation begins to become

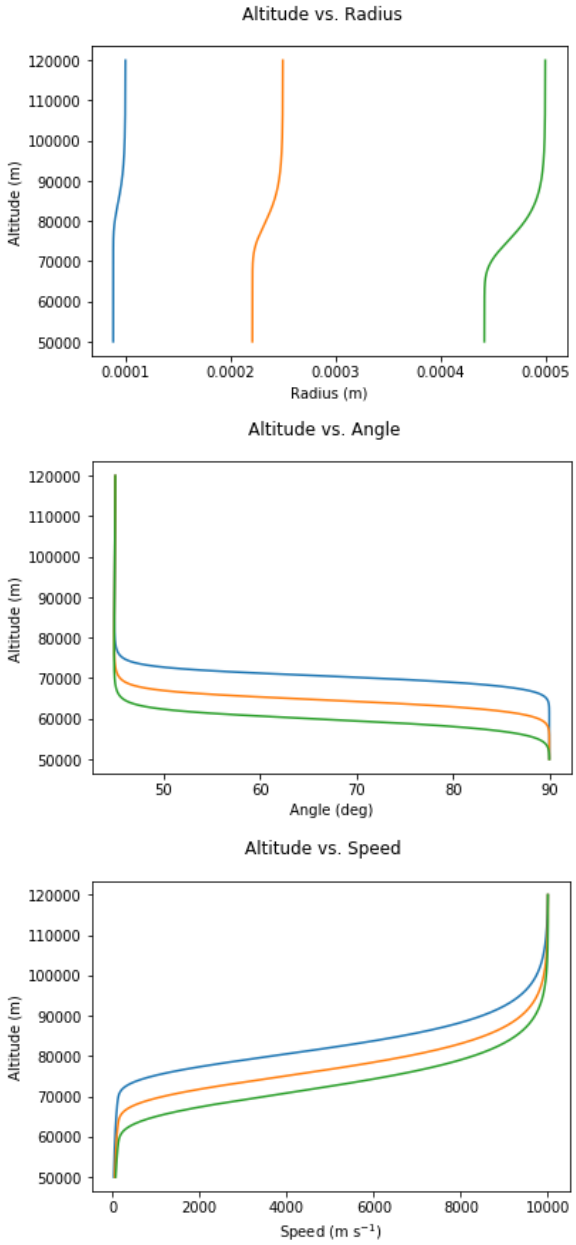

Figure 7. Results for a simulation of micrometeorites. These plots ablation (change in radius) with altitude, change in trajectory angle with altitude, and change in speed with altitude.

important around 90 km compared to 40 km. This reinforces the importance of the need for an accurate density model for higher altitudes, even though the density is essentially zero beyond a certain point, the impact that the density function has on the modeling equations is certainly nonzero. Note also when terminal velocity is reached, $z \simeq 50 - 70$ m.

We also should consider what happens when the angle of the trajectory θ is varied. The results of the simulations show that, for vertical trajectories, the micrometeorites are able to penetrate lower into the atmosphere before noticeable deceleration, and experience a shorter duration of deceleration. Vertical trajectories also correspond to more intense heating. For shallower trajectories, the micrometeorites slow down at higher altitudes, have a longer period of deceleration, and experience less intense heating.

7. Preliminary Thermal Analysis

We are now able to consider a preliminary heating model for the micrometeorites encountered, for example, in Section 6. This model is simply an order of magnitude estimate for an extreme case, assuming that all of the energy loss goes into heating the micrometeorite from radiative heat transfer from the shock wave. This will require a value of time duration for a heat pulse, which can be found from Figure 6. We first need to relate the total energy E_T to the temperature. We define the total energy per unit mass to be

$$e_t = C_v t + \frac{1}{2}v^2 + \phi,$$

and integrate over some control volume Ω to obtain

$$E_T = mC_v T.$$

As an example, consider a micrometeorite with $r = .001$ m with $\rho_m = 3000$ kg m^{-3}. Then, m is on the order of 10^{-5}. From the plot of dKE/dt, there is a heating pulse of roughly -35 J s^{-1} for 2 s. Therefore, an estimate for values of T are

$$T \sim \frac{70 \text{ J s}^{-1}}{10^{-5} \text{ kg} \cdot 1000 \text{ J kg}^{-1} \text{ K}^{-1}} \sim 7 \times 10^3 \text{ K}.$$

This discussion can be refined even further, however. Assume that the initial kinetic energy is equal to the final thermal energy of the micrometeorite, which again is a limiting case as much of this thermal energy would be lost due to radiation, but in this case, we have

$$\frac{1}{2}mv_0^2 = mC_v T_f.$$

Solve for T to show that

$$T_f = \frac{v_0^2}{2C_v}.$$

This tells us that the final temperature would be independent of the mass of the micrometeorite, which is an interesting result.

Now, how would we consider the time needed for heat to diffuse through the micrometeorite? For a semiinfinate slab, this is found by the time-diffusion approximation

$$t \simeq \frac{\ell^2}{\alpha}$$

where ℓ is the distance from the surface of the slab to the point within the surface. For spherical geometry, this is approximated by

$$t \simeq \frac{r^2}{3\alpha},$$

These time scales are still around 1 to 2 seconds, which is consistent with the results obtained from our simulations.

We also need to consider the technique discussed in [19]. That is, consider solutions to the integral equation

$$T(r,t) = \frac{2T_0}{\sqrt{\pi}} \int_{\frac{r}{2}(\kappa_H t)^{-1/2}}^{r} \exp(-\mu^2)\, d\mu,$$

which would also give us a temperature distribution inside the micrometeorite which is time-dependent. We obtain a preliminary thermal distribution from a finite element analysis using the COMSOL multiphysics program (reference: www.comsol.com). Results of a COMSOL simulation are given in the following figure.

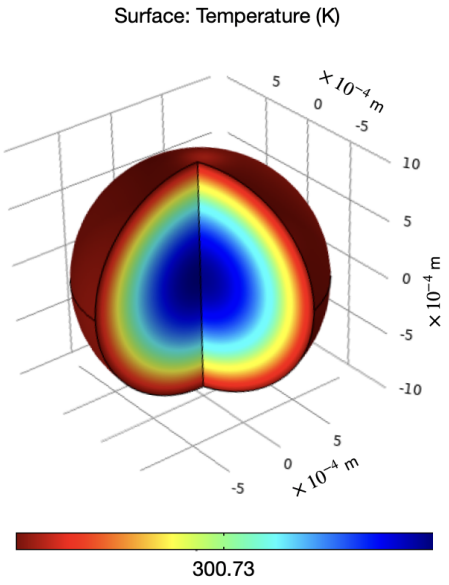

Figure 8. Temperature distribution profile inside a $r = 1.0$ mm micrometeorite at $t = .17$ s into a 2 s duration heat pulse with a maximum temperature of 2000 K.

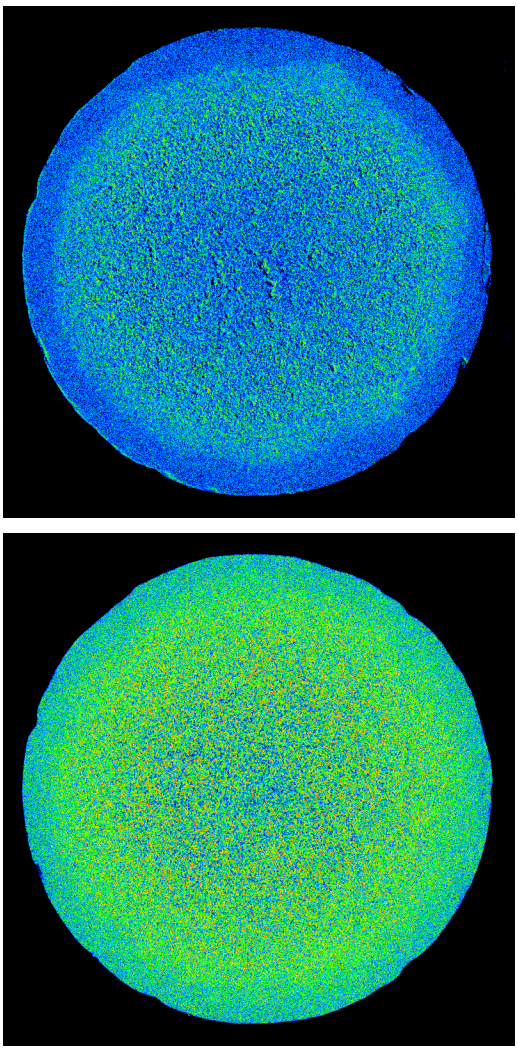

Figure 9. Compositional variation inside micrometeorites using backscatter imaging from the electron microprobe facility in the Department of Earth and Environmental Sciences at the University of Minnesota. Micrometeorite samples collected by Scott Peterson; images courtesy of Dr. Anette von der Handt.

8. Concluding Remarks

In this paper, we have established a complete micrometeorite trajectory analysis using a Python simulation. We have also discussed a preliminary thermal analysis, which acts as the foundation for future work. We can conclude a couple of interesting observations as a result of this study. First, that some micrometeorites with sizes on the order of 100 μm melt in their passage through the atmosphere, while others don't reach high enough temperatures to do so. Second, we predict that total

heating (> 2000 K) and time duration (> 1 s) is consistent with melting observed in some micrometeorites. We will make this more concrete in future work.

The results of this research also establish that, for vertical trajectories, the micrometeorites penetrate lower into the atmosphere before experiencing noticeable deceleration, and the duration of this deceleration is small. We also can see that vertical trajectories correspond to more intense heating. For shallower trajectories, micrometeorites slow down at higher altitudes, have a longer period of deceleration, and experience less intense heating.

Acknowledgments

I would like to offer my profound thanks to my research advisors, Dr. Paul Thomas and Dr. Phillip Ihinger for their guidance and support throughout this project. Their helpful comments through the model development stages and the writing of this paper can not go without recognition, not to mention the brilliant scientific discussions we shared. I deeply thank the both of them. I would also like to thank Dr. Ying Ma for his tremendous help with the COMSOL analysis, I look forward to continued work with him.

I also would like to acknowledge the work of Dr. Anette von der Handt from the University of Minnesota for providing us with images of micrometeorites under an electron microprobe, and I would like to thank Scott Peterson of New Hope, Minnesota, for collecting these samples.

The McNair Program at the University of Wisconsin-Eau Claire I thank as well, for providing me with support on many levels during my time as an undergraduate student. I also would like to thank the Office of Research and Sponsored Programs (ORSP) and the MIT Office of Graduate Education for providing me with funding to make this project possible.

References

[1] Alla, H., Freiner, S., and Carmes-Roques T. (2011). A computational fluid dynamics model using the volume of fluid method for describing the dynamics of spreading of Newtonian fluids. *Colloids and Surfaces A: Physicochemical and Engineering Aspects, 386*(1-3), 107-115.

[2] Andrey, K., Andrey, K., Efim, P., Vadim, K., and Elena T. (2017). Numerical modeling of the 2013 meteorite entry in lake Chebarkul, Russia. *Natural Hazards and Earth System Sciences, 17*(5), 671-683.

[3] Biberman, L.M., S. Ya. Bronin and M. V. Brykin. (1908). Moving of a blunt body through a dense atmosphere under conditions of severe aerodynamic heating and ablation. *Acta Astronautica, 7*, 53-65.

[4] Borovička, J. et al. (2013). The Košice meteorite fall: Atmospheric trajectory, fragmentation, and orbit. *Meteoritics & Planetary Science, 48*(10).

[5] Bronshten, V.A. (1983). Physics of Meteoritic Phenomena. Reidel, Dordrect.

[6] Brown, P.G. et al (2019). The Hamburg meteorite fall: Fireball trajectory, orbit, and dynamics. *Meteoritics & Planetary Science, 54*(9), 2027-2045.

[7] Carrillo-Sánchez, S.D., Nesvorný, D., Pokorný, P., and Plane, J.M.C. (2016). Sources of cosmic dust in the Earth's atmosphere. *Geophysical Research Letters, 43*(23).

[8] Chyba, C., Thomas, P., and Zahnle, K. (1993). The 1908 Tunguska explosion: Atmospheric disruption of a stony asteroid. *Nature, 361*, 40-44.

[9] Chyba, C., Thomas, P., Brookshaw, L., and Sagan, C. (1990). Cometary delivery of organic molecules to the early Earth. *Science, 249*(4967), 366-373.

[10] Gavrilov, A. Yu, and Lebedev, M.G. (2018). Determination of meteorite trajectories: Observations and modeling. *Computational Mathematics and Modeling, 29*(3), 265-274.

[11] Genge, M.J., Engrand, C., Gounelle, M., and Taylor, S. (2016). The classification of micrometeorites. *Meteorites & Planetary Science, 43*, 497-515.

[12] Ivanov, B. (2005). Numerical modeling of the largest terrestrial meteorite craters. *Solar System Research, 39*(5), 381-409.

[13] Jursa, A.S. (1985). Handbook of Geophysics and the Space Environment. *U.S. Department of Energy & Office of Scientific and Technical Information.*

[14] Kou, S. (1996). Transport Phenomena and Materials Processing. New York: Wiley.

[15] Larsen, J. (2019). On the Trail of Stardust: The Guide to Finding Micrometeorites: Tools, Techniques, and Identification.

[16] Liu, G.R., and Liu, M.B. (2003). Smoothed particle hydrodynamics, a meshfree particle method. World Scientific Publishing.

[17] Maurette, M. (2006). Micrometeorites and the mysteries of our origins. Berlin, NY: Springer.

[18] Passey, Q.R., and H.J. Melosh. (1980). Effects of atmospheric breakup on crater field formation. *Icarus, 42*. 211-233.

[19] Podolak, M., Pollack, J.B, and Reyonolds, R.T. (1978). Interactions of Planetesimals with Protoplanetary Atmospheres. *Icarus, 73*. 163-179.

[20] Springel, V. (2010). Smoothed particle hydrodynamics in astrophysics. *Annual Review of Astronomy and Astrophysics, 48*, 391-430.

[21] Teyssier, R. (2015). Grid-based hydrodynamics in astrophysical fluid flows. *Annual Review of Astronomy and Astrophysics, 53*, 235-364.

[22] Zingale, M. (2013). Pyro: A teaching code for computational astrophysical hydrodynamics. *Astronomy and Computing, 6*, 52-56.